5
Thermal Effects in Microscales

In this chapter we consider heat transfer in gas microflows. In the first section we concentrate on the thermal creep (transpiration) effects that may be important in channels with tangential temperature gradients on their surfaces. For example, a microchannel surface with a prescribed heat flux is subject to temperature variations along its surface, and this results in thermal creep flow. We analyze thermal creep with numerical simulations to demonstrate the main concept, and subsequently we describe a prototype experiment. In the second and third sections we study other temperature-induced flows and investigate the validity of the heat conduction equation in the limit $\mathrm{Kn} \to 0$. In the fourth and fifth sections we investigate the combined effects of thermal creep, heat conduction, and convection in pressure-, force-, and shear-driven channel flows.

5.1 Thermal Creep (Transpiration)

It is possible to start rarefied gas flows due to tangential temperature gradients along the channel walls, where the fluid starts creeping in the direction *from cold toward hot*. This is the so-called thermal creep or transpiration phenomenon. We explain this counterintuitive effect with the following example: Consider two containers filled with the same gas that are kept at the same pressure

$$P_1 = P_2$$

but at different temperatures

$$T_1 > T_2.$$

If these two containers are connected with a relatively thick channel ($\lambda \ll h$), the equilibrium condition requires no-flow in the channel. If the channel thickness (h) becomes comparable to the mean free path (λ), rarefied gas effects have to be taken into account. In such a case the local equilibrium mechanism is very complex, and interaction of the gas molecules with the walls must also be considered. Here, we consider free-molecular flow conditions (i.e., $\lambda \gg h$) to simplify the discussion. In this flow regime, the intermolecular collisions are negligible compared to the interaction of molecules with the surfaces. If we assume that molecule–wall interactions are *specular* (i.e., $\sigma_v = 0$), then the following analysis is valid. We assume that the density of the fluid is proportional to the number density (number of molecules per unit volume),

$$\rho \propto n,$$

and the temperature of the fluid is proportional to the square of average molecular speed,

$$T \propto \bar{c}^2.$$

The mass fluxes at the hot and the cold ends of the channel are

$$mn_1\bar{c}_1 \quad \text{and} \quad mn_2\bar{c}_2,$$

respectively; here m is the mass of the gas molecules. Then

$$\frac{mn_1\bar{c}_1}{mn_2\bar{c}_2} \approx \frac{\rho_1}{\rho_2}\left(\frac{T_1}{T_2}\right)^{0.5} = \frac{P_1}{P_2}\left(\frac{T_2}{T_1}\right)^{0.5} = \left(\frac{T_2}{T_1}\right)^{0.5} \leq 1,$$

where we have used the equations of state

$$P = \rho RT \quad \text{and} \quad \frac{P_1}{P_2} = 1.$$

The above analysis indicates a **flow creeping from cold to hot**. Osborne Reynolds was the first to realize this phenomenon, and he coined the term *thermal transpiration* (Reynolds, 1879). At about the same time, Maxwell developed independently a theory for thermal creep. In the early 1900s, Knudsen built a molecular compressor based on the thermal transpiration idea by connecting a series of tubes with constrictions arranged between each tube (Knudsen, 1910a; Knudsen, 1910b). The constrictions were very small, so that the rarefaction effects became important in the constrictions. By heating the same side of these constrictions to very high temperatures (773 K), Knudsen was able to maintain considerable pressure gradients

(Loeb, 1961). According to (Ebert and Albrand, 1963), Gaede also described a *thermal pump* in his unpublished notes. Other developments in thermal creep driven vacuum pumps can be found in (Vargo et al., 1998).

A detailed derivation of thermal creep boundary condition for rarefied flows with $\lambda < h$ is given in (Kennard, 1938; Loeb, 1961). It can also be derived directly from the Boltzmann equation (see Section 15.4.2). In order to accommodate the thermal creep effects, the wall velocity is enhanced with the following term:

$$U_{\mathrm{c}} = \frac{3}{4}\frac{\mu R}{P}\frac{\partial T}{\partial s}, \tag{5.1}$$

where U_{c} is the creep velocity, and $\frac{\partial T}{\partial s}$ is the tangential temperature gradient along the surface. Therefore, the high-order velocity slip boundary condition is modified as

$$U_s = \frac{1}{2}\left[(2-\sigma)U_\lambda + \sigma U_w\right] + U_c.$$

The velocity profile for a pressure-driven channel flow of thickness h, including the thermal creep effects, is then given by equation (4.5) with (5.1) added on to the right-hand side. Integrating this profile, we obtain the mass flowrate:

$$\dot{M} = -\frac{h^3 P}{12\mu RT}\frac{dP}{dx}\left[1 + 6\frac{2-\sigma_v}{\sigma_v}(\mathrm{Kn} - \mathrm{Kn}^2)\right] + \frac{3}{4}\frac{\mu h}{T}\frac{dT}{dx}. \tag{5.2}$$

We conclude that thermal creep can change the mass flowrate in a channel. If the pressure gradient and the temperature gradient along the channel walls act along the same direction, the flowrate is decreased; otherwise, the flowrate is increased.

- *Therefore, it is possible to have nonzero flowrate in a microchannel even in the case of zero pressure gradient.*

5.1.1 Simulation Results

An interesting aspect of thermal creep is that it causes zero net mass flowrate in channels where thermal creep and pressure gradient balance each other. To demonstrate this we simulated air flow in microchannels of various dimensions connecting two tanks kept at different conditions with

- Temperatures at 300 K and 400 K, and
- Knudsen number at Kn = 0.365, 0.122, 0.052.

The pressure in both tanks is initially atmospheric. Thermal creep effects cause pumping of the fluid toward the hot tank, increasing the pressure in the hot tank and lowering the pressure in the colder one. This pressure

TABLE 5.1. Pressure differences due to the thermal creep effects obtained by numerical simulation and from the analytical formula.

Gas	$\overline{\mathrm{Kn}}$	$\Delta P_{\mathrm{analy}}(Pa)$	$\Delta P_{\mathrm{numer}}(Pa)$
Air	0.052	342.0	336. 0
Air	0.122	1482.0	1409.0
Air	0.365	9151.0	8832.0

difference eventually starts flow in the middle of the channel in the direction from hot to cold (high pressure to low pressure), resulting in zero average mass flowrate in the channel as the steady state is reached. For zero net mass flowrate, equation (5.2) can be written as

$$\frac{dP}{dx} = \left(\frac{9\mu^2 R}{h^2 P}\right) \frac{\frac{dT}{dx}}{1 + 6[\frac{2-\sigma}{\sigma}(\mathrm{Kn} - \mathrm{Kn}^2)]}.$$

It is possible to integrate this equation approximately using *average* values of viscosity ($\bar{\mu}$), pressure ($\bar{P} = \frac{P_1+P_2}{2}$), and Knudsen number ($\overline{\mathrm{Kn}}$), resulting in

$$P_1 - P_2 \approx \left(\frac{9\bar{\mu}^2 R}{h^2 \bar{P}}\right) \frac{(T_1 - T_2)}{1 + 6\left(\frac{2-\sigma}{\sigma}\left(\overline{\mathrm{Kn}} - \overline{\mathrm{Kn}}^2\right)\right)}, \tag{5.3}$$

where viscosity and Knudsen number are evaluated at average temperature ($\bar{T} = \frac{T_1+T_2}{2}$) and average pressure ($\bar{P}$). Equation (5.3) shows that the pressure drop between two tanks can be increased by either decreasing the channel thickness (h) or the average pressure ($\bar{P}$). In other words:

- *Thermal creep effects can be significant in rarefied flows where the pressure is low or in microflows in atmospheric pressures where the typical dimensions are on the order of a micron or lower.*

The steady-state pressure distribution along the channel center and in the reservoirs, normalized with atmospheric pressure (initial pressure at both tanks), is given in Figure 5.1 for three different channel sizes. It is seen that the pressure change due to thermal creep for high Kn flows is nonnegligible. In Table 5.1, we compare the pressure differences predicted by equation (5.3) with the numerical values obtained by simulations; the agreement is very good.

The above numerical experiment describes an unsteady problem for which the relevant time scales are governed by two different transient processes. The *first transient process* is due to the fluid starting to creep along the channel surface. As time goes on, the creeping fluid layer starts interacting with the stagnant fluid layers above it, creating a boundary layer similar to the impulsively started wall problem, the so-called Rayleigh problem (Batchelor, 1998). Of course, formation of the boundary layer creates

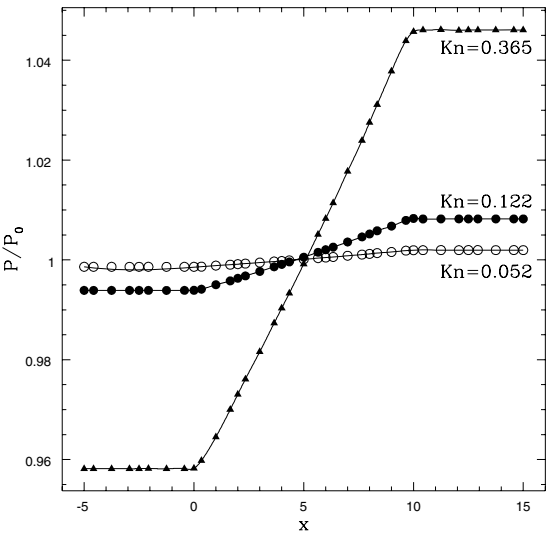

FIGURE 5.1. Normalized pressure variation along the channel center and reservoirs for different rarefaction parameters ($P_0 = 1\,atm$). Triangles and circles show the location of calculation points.

shear stresses, which, in turn, activate the velocity slip mechanism (Kennard, 1938). This is the initial transient process with time scale

$$t \propto \frac{h^2}{\nu}.$$

Considering microchannels with typical height of about one micron, this transient is very fast.

The *second time scale* of the problem corresponds to the time it takes to get from initial transients to a steady-state solution where the net mass flowrate is zero. This time scale is based on the creep velocity and tank dimensions. In particular, this time scale increases as the tank size is increased. In the limit where the tanks are reservoirs of infinite dimensions, the fluid steadily creeps from the cold to the hot tank, and the pressure at the two reservoirs remains practically the same.

Figure 5.2 shows the flow field for early times as well as for a steady-state behavior. A uniform flow is obtained in the channels initially (past the end of the aforementioned first process). As more fluid is introduced into the hot tank, the pressure there increases while the pressure at the cold tank decreases. Initially, the pressure built up by this process is not sufficient to reverse the flow in the middle of the channel, and more fluid is being transported into the hot tank (see Figure 5.2 (a)). When the pressure in the hot tank is sufficiently high to overcome the flow due to thermal creep, the

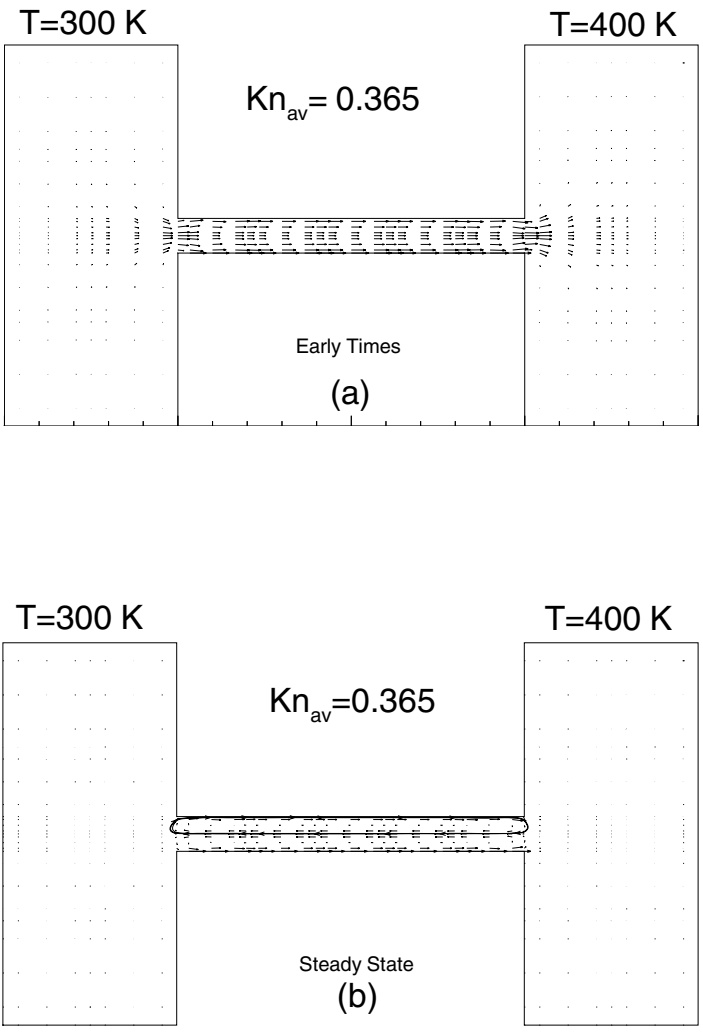

FIGURE 5.2. Demonstration of the thermal creep effects: Flow field for early times (a), and steady-state solution (b) ($\overline{\mathrm{Kn}} = \mathrm{Kn}_{\mathrm{av}} = 0.365$).

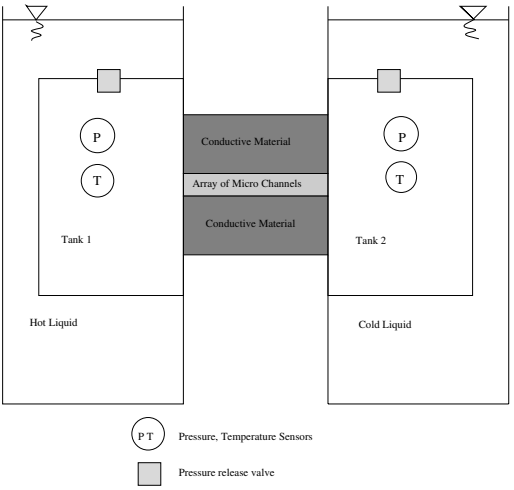

FIGURE 5.3. Proposed experimental apparatus for studying thermal creep effects.

net mass flowrate across the channel becomes zero, and the steady solution is obtained; this is shown in Figure 5.2 (b). A single streamline passing through the channel center is also shown in the plot. It is seen that the fluid recirculates in the channel and there is no net flow to either tank.

This pumping effect of thermal creep has been exploited by (Sone et al., 1996b), who designed a channel with periodic ditches, similar to the grooved channel of Figure 3.25 but with the groove present on both walls. They imposed a periodic temperature variation, whereby the temperature *decays* linearly on the groove side, but it *increases* linearly on the channel wall. This device produces a unidirectional flow with maximum mass flowrate at Kn ≈ 0.3, and it works both for channels as well as pipes. While the original studies in (Sone et al., 1996b), were based on DSMC, subsequently an experiment was conducted to verify the pumping effect (Sone et al., 2001).

5.1.2 A Thermal Creep Experiment

The purpose of this experiment is to examine the importance of thermal creep effects in microchannel flows. It is based on the numerical example presented above, also in (Beskok et al., 1995), and ideas similar to Knudsen's experiments (Loeb, 1961), but it differs from the early experiment of (Vargo and Muntz, 1996), where porous diaphragms were used rather than microchannels.

The objective is to test the thermal creep effects in an apparatus presented schematically in Figure 5.3. It consists of two reservoirs connected through a series of microchannels made out of silicon. The typical dimen-

sions of the microchannels should be 1 μm thick, 100 μm wide, and few millimeters long. Using a series of microchannels increases the net flow area without effectively increasing the channel area to perimeter ratio.

A possible experimental procedure is as follows: *First*, both of the pressure release valves are open, and therefore, the system is in equilibrium with the ambient conditions. Then, the pressure release valves are closed. The temperature and the pressure of the system are recorded to ensure that the two reservoirs are at identical thermodynamic state. *Second*, the reservoirs are dipped into constant-temperature fluid baths at different temperatures T_1 and T_2. The pressure and the temperature in the reservoirs should be recorded in time. If the continuum hypothesis is valid, the pressure in the reservoirs should be unchanged. If thermal creep effects are present, the pressure in the cold reservoir should decrease, and the pressure in the hot reservoir should increase. The experiments should run until a stationary state is observed. The time scale of the experiment is directly related to the size of the reservoirs. Therefore, the reservoirs should be designed as small as possible. However, they should be large enough to maintain continuum description for the gas in them (i.e., $\mathrm{Kn} < 0.001$). It is possible to increase the rarefaction effects in the experiments by performing the experiment at lower pressures than atmospheric conditions. Therefore, a systematic study of thermal creep as a function of Kn can be performed. Also, the temperature of the fluid baths can be changed from one experiment to another in order to verify the sensitivity of thermal creep to temperature gradients for a given Kn.

5.1.3 Knudsen Compressors

Micromolecular compressors are useful for various microscale gas pumping applications. For example, compressors pumping gas samples through micromass spectrometers can be used to detect pollutants and various chemical or biological agents. MEMS-based thermal transpiration Knudsen compressors were proposed in (Pham-van-Diep et al., 1995), and in (Beskok et al., 1995). The idea in (Pham-van-Diep et al., 1995), is based on utilization of a cascade of multiple stages to obtain large pressure variations. Each stage consists of an array of capillaries and a connector section. The temperature increase imposed along the capillary pumps the gas from cold toward the hot direction, resulting in pressure increase in the capillary section. The gas is cooled in the connector section, and thus the temperature drops to the value corresponding to the inlet of the capillary section. This creates periodically repeatable temperature variations in each stage of the compressor. Since the pressure in the connector section drops only slightly, it is possible to have a net pressure built up with multistage units.

Large-scale Knudsen compressors have low volumetric flowrate and inefficient energy usage; however, their microscale counterparts eliminate these disadvantages and result in low-power gas-pumping systems with nonmov-

ing components. (Vargo et al., 1998) built a microvacuum pump delivering 5×10^{14} molecules per second with a pump volume of 0.16 mL at inlet pressure of 10 mTorr and power input of 28.5 mW. Another micro pump with the same flowrate was built to operate at 1 mTorr. It required a volume of 13.9 mL and power input of 2.4 W. A tenfold decrease in the inlet pressure resulted in almost a hundred times increase in the power input and the volume of the system. The flow in the capillary section of the Knudsen compressor is in transition or free-molecular flow regime, and thus the capillary radius is small, and thermal transpiration effects are dominant in this section. However, the dimensions of the connector section are considerably larger than the local mean free path, so that slip or continuum flow is present in this section. In the compressor built by Vargo et al., the capillary and the connector radii were 0.225 μm and 10.795 mm, respectively. The bottleneck in the design of a Knudsen compressor is usually in determining the dimensions of the connector section, which becomes a limitation for low-pressure applications where the mean free path is already quite large.

In the experiments of Vargo et al., the maximum temperature variation in one stage of the compressor was about 20 to 30 K, with average temperature of 282 K. The inlet pressure and the working gas were varied. Good device performance for pressures as low as 1 mTorr was reported. Finally, Vargo et al. have developed a numerical model for predicting flowrate and pressure buildup in Knudsen compressors operating in the transition flow regime. The numerical predictions were validated using the experimental data, and the new algorithm was employed to study compressor performance under various flow conditions.

5.2 Other Temperature-Induced Flows

In addition to the flow induced by thermal creep, which is an $\mathcal{O}(Kn)$ effect, there are other possibilities for setting up a flow in rarefied flows in the absence of any external forces, e.g., gravity. Here we list a few representative cases and provide a short explanation:

- thermal stress slip flow,
- nonlinear thermal stress flow,
- flow induced around the edge of a heated plate, and
- flow induced by a temperature discontinuity.

Most of these cases were discovered by Sone, Aoki, and their collaborators by analyzing the Boltzmann equation (see Section 15.4.2). They are most probably present in microsystem flows, but they are difficult to isolate and be detected as individual effects. Here we give a brief summary for each following the work in (Sone, 2002; Sone, 2000).

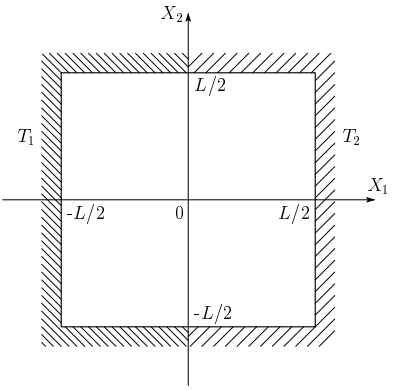

FIGURE 5.4. Flow domain showing the temperature discontinuities at the upper and lower walls. (Courtesy of K. Aoki.)

The **thermal stress slip flow** is an $\mathcal{O}(\mathrm{Kn}^2)$ effect, and it is derived following a consistent second-order expansion in Kn of the Boltzmann equation. In that case, in addition to the thermal creep that is present in the first-order expansion of the boundary terms, there is a correction term for the slip velocity proportional to the *normal gradient* of the temperature. A nonuniform normal gradient can cause a slip velocity even if the boundary is isothermal. To explain this in more detail, we follow the argument of Sone (see Section 15.4.2 and (Sone, 2002)). Let us consider a gas between two eccentric circular cylinders with different uniform temperatures T_1 and T_2. No thermal creep flow is induced; however, there is, in general, a nonuniform normal temperature gradient on each cylinder, that is,

$$\frac{\partial^2 T}{\partial x_i \partial x_j} n_i t_j \neq 0,$$

where n_i and t_j are components of the unit vectors in the normal and tangential directions, respectively. A global flow is then set up circulating between the cylinders along the clockwise direction if the temperature of the outside cylinder T_2 is higher. This phenomenon was discovered by (Sone, 1972), who termed it "thermal stress slip flow."

The **nonlinear thermal stress flow** is an $\mathcal{O}(\mathrm{Kn})$ effect and was discovered by (Kogan et al., 1976) as a new type of convection. When the temperature gradient in a gas is so large that its nonlinear effect is not negligible, the thermal stress does not balance by itself and remains in the momentum equation (see momentum equations in Section 15.4.2). This causes a flow when the distance between isothermal lines or surfaces varies along them. In this flow, in contrast to the thermal creep flow and thermal stress slip flow, a solid boundary plays only an indirect role in setting up the isothermal contours.

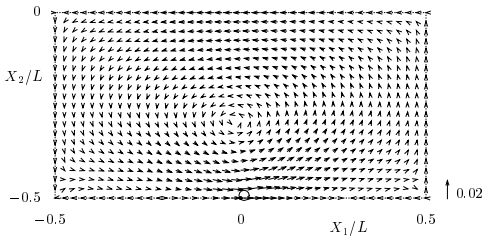

(a) Kn = 0.2

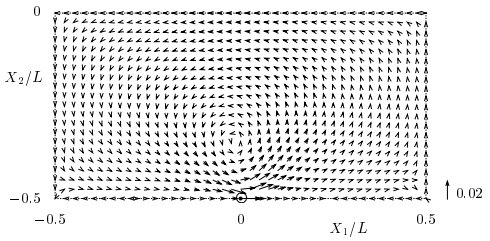

(b) Kn = 0.02

FIGURE 5.5. Flow induced in the lower half of the domain for $T_2/T_1 = 2$. The scale $\sqrt{u^2+v^2}/\sqrt{2RT_1} = 0.02$ is indicated next to the plots. The upper plot corresponds to Kn = 0.2 and the lower plot to Kn = 0.02. (Courtesy of K. Aoki.)

The **flow induced around the sharp edge of a heated plate** cannot be predicted by the asymptotic analysis of the Boltzmann equation as in the previous two cases. This phenomenon was discovered more recently in numerical and experimental work by (Aoki et al., 1995) and (Sone and Yoshimoto, 1997). If a uniformly heated plate is placed in the middle of gas contained in a tank of uniform temperature, flow is induced around the edge of the plate for a wide range of Knudsen number. There is no flow induced by thermal creep, since the temperature is uniform everywhere. The induced velocity scales approximately as $\mathcal{O}(\sqrt{\mathrm{Kn}})$.

Lastly, **flow induced by a temperature discontinuity** has been studied by (Aoki, 2001), who set up a flow in a square enclosure, half of which is at temperature T_1 and the other half at temperature T_2 (see Figure 5.4). A flow is induced from the colder to the hotter part along the one wall with the discontinuity at the middle, and this sets up a global circulating flow (see Figure 5.5). The maximum flow speed tends to a constant value at low Kn values and decays for $\mathrm{Kn} \geq 0.1$.

5.3 Heat Conduction and the Ghost Effect

We examine here the possible breakdown of the heat conduction equation in the limit that $\mathrm{Kn} \to 0$. This phenomenon was studied by (Sone et al.,

1996a) and shows a fundamental inconsistency in the momentum and energy (Navier–Stokes) equations. We consider a gas at rest contained in a tank. According to the continuum description, the gas temperature field is described by the heat conduction equation, i.e., the energy equation with all the convective terms absent. Below, we follow the argument of (Sone, 2002; Sone, 2000), that demonstrates that the heat equation is not always appropriate, e.g., in microscales.

Let us consider the energy equation in the continuum limit and examine only the relevant terms (for a monoatomic gas) as follows:

$$\frac{5}{2}\rho u_i \frac{\partial(RT)}{\partial x_i} = \cdots + \frac{\partial}{\partial x_i}\left(k\frac{\partial T}{\partial k_i}\right), \tag{5.4}$$

where k is the thermal conductivity. The corresponding heat conduction equation for a gas at rest is

$$\frac{\partial}{\partial x_i}\left(k\frac{\partial T}{\partial x_i}\right) = 0.$$

The thermal conductivity (k) of a gas is a function of its mass as well as its temperature. Specifically, k (divided by the density of the gas) is proportional to the mean free path with the proportionality coefficient a general function of temperature, i.e.,

$$\frac{k}{\rho} = \mathcal{F}\left(\frac{T}{T_0}\right)\sqrt{2RT}R\lambda.$$

Therefore, in the energy equation the conduction term divided by the density is $\mathcal{O}(\lambda)$. For a gas flow of the order of the mean free path (λ), which is neglected in classical gas dynamics, its convection term is of the same order as the conduction term and cannot be neglected. More specifically, the order of magnitude for the *convection* term is

$$\text{Convection} \propto \mathcal{O}(\rho V RT/L),$$

and the order of magnitude for the *conduction* term is

$$\text{Conduction} \propto \mathcal{O}(\rho(RT)^{3/2}\lambda/L^2),$$

where V and L are, respectively, the characteristic flow speed of the gas and the length scale of variation of the temperature of the gas. Thus, the two terms are comparable when

$$V \propto \mathcal{O}(\sqrt{RT}\lambda/L) \propto \mathcal{O}(\text{Kn}).$$

The question then is whether there are flows of such magnitude; however, we have already seen in this section that both the thermal creep flow and the nonlinear thermal stress flow are possible candidates. These flows are

always present, even at extremely small Knudsen numbers, unless all surfaces in the device have uniform temperature *and* all temperature isocontours are parallel. These two conditions are difficult to satisfy simultaneously except in the trivial case of two infinite plates at exactly uniform temperatures with no end effects! Therefore, according to (Sone, 2002) the heat-conduction equation is inappropriate for describing the temperature field of a stationary gas in the continuum limit.

Sone termed this the "ghost effect" in the sense that something that does not exist in the world of a gas in the continuum limit has a finite effect in the molecular world. In (Sone, 2000) an example of the ghost effect is given for a channel with small periodic temperature variation at the two walls. No experiments in microscales have reported the ghost phenomenon, and it is difficult to assess its practical significance; nevertheless, it is a significant result from the fundamental principles point of view.

5.4 Heat Transfer in Poiseuille Microflows

It is possible to create Poiseuille flow in a microchannel using either a pressure drop or a body force. Although the continuum descriptions for both cases are similar, kinetic theory predictions and statistical simulations for force-driven flows show that the Navier–Stokes solutions fail to predict the important temperature minimum effects, even for $\mathrm{Kn} \approx 0.01$ flows with $M < 0.1$ (Zheng et al., 2002). Therefore, we divide this section into two parts, addressing the pressure- and force-driven flows separately.

5.4.1 Pressure-Driven Flows

Heat transfer in pressure-driven gas microflows has important engineering applications. There have been several studies of microflows under constant wall temperature and heat flux conditions. For example, thermally developing slip flows under constant heat flux have been presented for circular and rectangular microchannels in (Ameel et al., 1997; Yu and Ameel, 2002), respectively. A similar problem is studied at the entrance of a conduit by including the heat transfer within the Knudsen layers (Chen and Xu, 2002). Thermally developing flows in circular tubes under constant wall temperature have been studied in the slip flow regime (Larrodé et al., 2000). The constant-temperature convective heat transfer under hydrodynamically and thermally fully developed conditions is considered for various geometries and flow regimes, such as slip flow in rectangular channels (Tunc and Bayazitoglu, 2002) and flow in two-dimensional channels for $0 < \mathrm{Kn} \leq 10$ (Simek and Hadjiconstantinou, 2002).

In this section, we neglect gas compressibility effects and present an analytical treatment of heat transfer for pressure-driven flows. We consider

the slip flow regime where the continuum description is valid. Such results were first obtained by (Inman, 1964), who showed that *reduced* heat transfer rates are obtained in the presence of slip flow. Specifically, Inman obtained the following equation for the Nusselt number Nu for constant heat flux q at the wall

$$\frac{1}{\mathrm{Nu(Kn)}} = \frac{17}{140} - \frac{9\,\mathrm{Kn} + 48\,\mathrm{Kn}^2}{35(1+6\,\mathrm{Kn})^2} + \frac{\gamma}{\gamma+1}\frac{\mathrm{Kn}}{\mathrm{Pr}}, \tag{5.5}$$

where the Nusselt number is defined as

$$\mathrm{Nu} \equiv \frac{qD_H}{k\Delta T}.$$

Here D_H is the hydraulic diameter ($D_H = 2 \times (2h) = 4h$ for a channel of total width $2h$), and ΔT is the temperature difference between the wall and the bulk of the fluid. Also, $\mathrm{Nu(Kn} = 0) = 8.235$ is the value corresponding to no-slip conditions. The above equation is based on Maxwell's first-order slip condition and neglects the effect of thermal creep.

Next, we analyze the combined effects of convection and thermal creep. The momentum equation subject to slip boundary conditions with a specified tangential temperature variation (see equation (2.19)) can be solved analytically. The rarefaction effects on momentum transfer can be investigated either by analyzing the volumetric flowrate increase in a pressure-driven channel or by analyzing the change in the skin friction coefficient for a fixed volumetric flowrate, under an appropriately specified pressure gradient. The nondimensional velocity distribution in a channel extending from $y = -h$ to $y = h$ is obtained as

$$\begin{aligned} U(y/h) = \frac{\mathrm{Re}}{2}\left|\frac{\partial p}{\partial x}\right| \left[1 - \left(\frac{y}{h}\right)^2 + 2\left(\frac{2-\sigma_v}{\sigma_v}\right)\frac{\mathrm{Kn}}{1+\frac{1}{2}\,\mathrm{Kn}}\right] \\ + \frac{3}{2\pi}\frac{(\gamma-1)}{\gamma}\frac{\mathrm{Kn}^2\,\mathrm{Re}}{\mathrm{Ec}}\frac{\partial T_s}{\partial x}, \end{aligned} \tag{5.6}$$

where $\frac{\partial T_s}{\partial x}$ denotes the tangential temperature variation along the channel surface, and we defined $\mathrm{Kn} = \lambda/h$, with h the half-channel width. Given this parabolic velocity profile we obtain the coefficient of high-order boundary condition from equation (2.39) to be $b = -\frac{1}{2}$. Correspondingly, the volumetric flowrate $\dot{Q}$ through the channel, in nondimensional form, becomes

$$\dot{Q} = \frac{4}{3} + 4\left(\frac{2-\sigma_v}{\sigma_v}\right)\frac{\mathrm{Kn}}{1+\frac{1}{2}\,\mathrm{Kn}} + \frac{3}{\pi}\frac{(\gamma-1)}{\gamma}\frac{\mathrm{Kn}^2\,\mathrm{Re}}{\mathrm{Ec}}\frac{\partial T_s}{\partial x}, \tag{5.7}$$

since $|\frac{\partial P}{\partial x}| = \frac{2}{\mathrm{Re}}$. The leading-order variation in the volumetric flowrate under fixed $\frac{\partial p}{\partial x}$ is *linear* in Kn due to velocity slip, and *quadratic* in Kn due

to thermal creep effects (for fixed Eckert number). However, since $\mathrm{Kn} \propto M/\mathrm{Re}$ and $\mathrm{Ec} \propto M^2$, then we see that the thermal creep term is linear in Kn, i.e., proportional to Kn/M.

In order to maintain zero average flowrate in a channel under a prescribed pressure gradient for an incompressible flow, the following condition should be maintained:

$$\frac{\partial p}{\partial x} = \frac{\frac{9}{2\pi}\frac{(\gamma-1)}{\gamma}\,\mathrm{Kn}^2\,\frac{\partial T_s}{\partial x}}{\mathrm{Ec}(1+3(\frac{2-\sigma_v}{\sigma_v})\frac{\mathrm{Kn}}{1+\frac{1}{2}\,\mathrm{Kn}})}. \tag{5.8}$$

In this case, if

$$\frac{\partial T_s}{\partial x} > 0,$$

the flow creeps from cold to hot along the channel surface, where a positive pressure gradient creates back-flow in the middle of the channel (Kennard, 1938; Loeb, 1961). With regard to the effects of thermal creep on Fanning friction coefficient of the flow for a fixed volumetric flowrate, the ratio of the friction coefficient of a slip surface C_f to the friction coefficient C_{f_0} of a no-slip surface is given by

$$\frac{C_f}{C_{f_0}} = \frac{1 - \frac{3}{\pi\dot{Q}}\,\mathrm{Kn}^2\,\frac{\mathrm{Re}}{\mathrm{Ec}}\,\frac{\partial T_s}{\partial x}}{1+3\frac{2-\sigma_v}{\sigma_v}(\frac{\mathrm{Kn}}{1+\frac{1}{2}\,\mathrm{Kn}})}. \tag{5.9}$$

It is seen that for fixed flowrate $\dot{Q}$, Eckert number Ec, and Reynolds number Re, the ratio of Fanning friction coefficients of slip flow to the no-slip flow changes significantly by varying the Knudsen number Kn. For flows without thermal creep effects (i.e., $\frac{\partial T_s}{\partial x} = 0.0$), the extra terms in the numerator of equation (5.9) are absent, and the formula is further simplified; see more details in (Beskok and Karniadakis, 1992; Beskok and Karniadakis, 1994).

The above analytical results can be used to validate computer programs for microfluidic applications. Here we present computations obtained with the spectral element program μ**Flow**. Comparisons are performed up to $\mathrm{Kn} = 0.15$, and the results are presented in Figure 5.6. The dashed line and the solid line show the *drag reduction* predicted by the first- and high-order slip flow theory without thermal creep effects, respectively. The triangles correspond to numerical predictions with high-order slip flow theory, and the circles correspond to numerical predictions with high-order slip flow theory including in this case the thermal creep effects (here $\mathrm{Ec} = 1.0$, $\mathrm{Re} = 1.0$, and $\frac{\partial T_s}{\partial x} = 1.0$). The differences between the analytical and numerical results are negligible.

The aforementioned simplified analysis can also be used to explain the drag reduction observed in the experiments reported in (Pfahler et al., 1991). For comparison, the experimental results are also plotted in Figure 5.6. The ratio predicted from equation (5.9) for $\mathrm{Kn} = 0.088$ corresponding

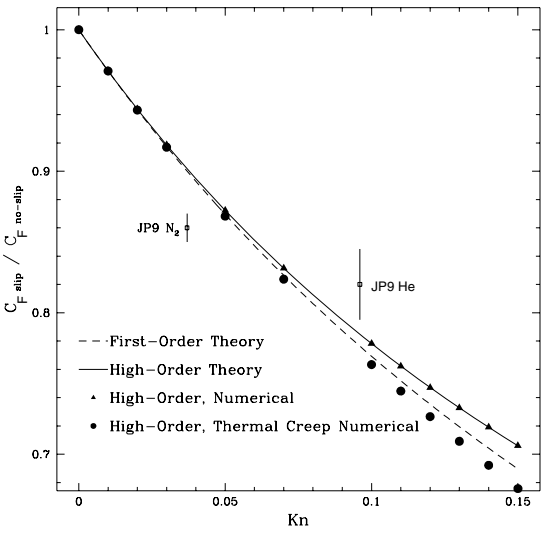

FIGURE 5.6. Ratio of Fanning friction coefficients of slip flow to no-slip flow in a pressure-driven channel. (Parameters for thermal creep contribution are Ec = 1.0, Re = 1.0, and $\frac{\partial T_s}{\partial x} = 1$.)

to the helium flow (case JP9 in (Pfahler et al., 1991)) is 0.79 in reasonable agreement with the measured value 0.8 to 0.85. The nitrogen flow gives a slightly greater drag reduction of about 0.86 compared to the theoretical predictions of 0.9 for Kn = 0.04. Our predictions assume accommodation coefficient $\sigma_v = 1$ and that compressibility effects in the channels are neglected. Thus, the Knudsen number variation in the channels due to compressibility effects is not taken into account, and the Knudsen number is calculated by taking the arithmetic average of the inlet and outlet Knudsen numbers of the microchannel. Furthermore, isothermal flow conditions are assumed, and thermal creep effects are neglected. For channel thicknesses significantly smaller, corresponding to Kn > 0.1, the experimental results show a strong dependence of the ratio of drag coefficients on the Reynolds number, which is not predicted by the above analysis.

Regarding heat exchange in microdomains, it is interesting to note that the viscous heating terms are quite significant; see also (Hadjiconstantinou, 2003b), for a discussion on shear work on solid boundaries for Kn ≤ 3. For example, if the reference temperature T_0 is taken to be the room temperature and the specified temperature difference of the domain ΔT is small, the viscous heating effects become nonnegligible for $M \geq 0.05$ (see equation (2.22)). An analytical solution of general heat convection problem for steady and thermally fully developed planar microchannel flows under specified uniform heat flux ($\dot{q}$) on the boundaries can be obtained by

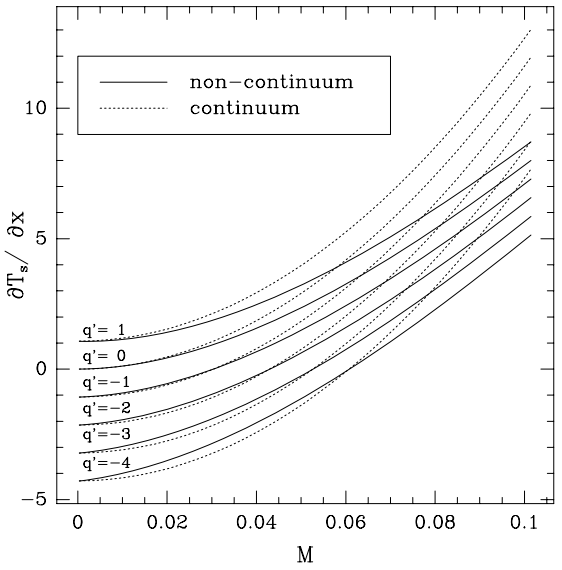

FIGURE 5.7. Variation of tangential temperature gradient ($\frac{\partial T_s}{\partial x}$) along the surface of a pressure-driven channel as a function of Mach number for different levels of heat fluxes ($\dot{q}$) (Re $= 1.0, \Delta T = 1\,\mathrm{K}$, and $T_0 = 300\,\mathrm{K}$).

decomposing the temperature profile into two parts,

$$T(x, y) = \frac{\partial T_s}{\partial x} x + \theta(y), \tag{5.10}$$

where $\frac{\partial T_s}{\partial x} x$ and $\theta(y)$ show the axial and cross-flow temperature variations, respectively. The coordinates x and y are also nondimensionalized here with the reference length scale. A global energy balance in the domain with an *insulated top surface* and a specified *constant heat flux* on the bottom surface gives the following relation for the tangential temperature gradient along the channel:

$$\frac{\partial T_s}{\partial x} = \frac{1}{\mathrm{RePr}\dot{Q}} \left(\dot{q} + \frac{8}{3} \mathrm{EcPr} \right). \tag{5.11}$$

The corresponding cross-flow temperature distribution in the channel is

$$\theta(y) = \mathrm{RePr} \frac{\partial T_s}{\partial x} \left(B \frac{y^2}{2} - \frac{y^4}{12} \right) - \mathrm{EcPr} \frac{y^4}{3} + Cy + D, \tag{5.12}$$

where

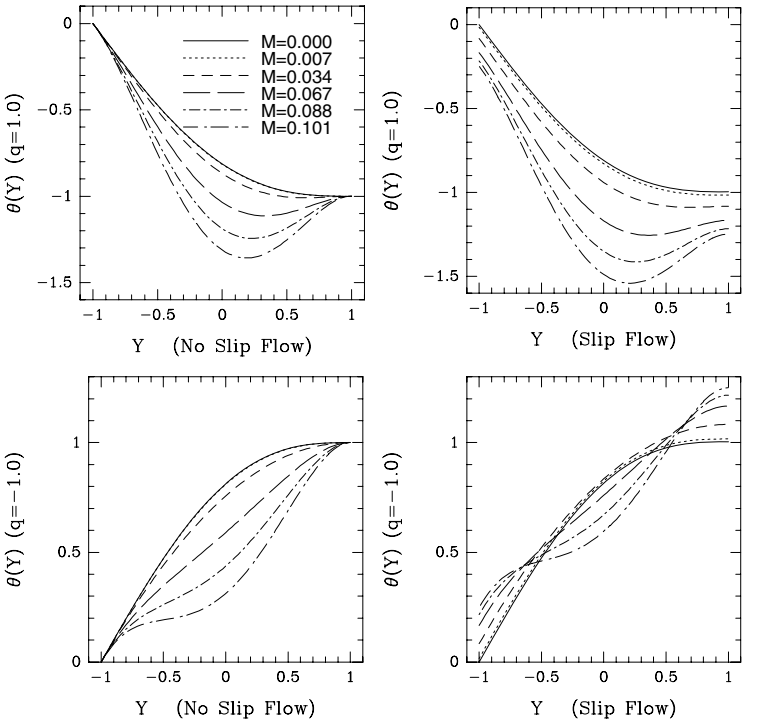

FIGURE 5.8. Variation of temperature profiles in a pressure-driven channel flow for continuum and rarefied flows, with specified heat flux on the bottom surface ($Y = -1$), as a function of Mach number ($\mathrm{Re} = 1.0$ and $\mathrm{Pr} = 0.7$).

$$B = 1 + 2\left(\frac{2-\sigma_v}{\sigma_v}\right)\frac{\mathrm{Kn}}{1+\frac{1}{2}\mathrm{Kn}} + \frac{3}{2\pi}\frac{(\gamma-1)}{\gamma}\frac{\mathrm{Kn}^2\,\mathrm{Re}}{\mathrm{Ec}}\frac{\partial T_s}{\partial x},$$
$$C = \mathrm{RePr}\frac{\partial T_s}{\partial x}\left(\frac{1}{3} - B\right) + \frac{4}{3}\mathrm{EcPr},$$
$$D = \theta_0 - \frac{2\gamma}{\gamma+1}\frac{\mathrm{Kn}}{\mathrm{Pr}}\dot{q} + \frac{5}{3}\mathrm{EcPr} - \mathrm{RePr}\frac{\partial T_s}{\partial x}\left(\frac{3}{2}B - \frac{5}{2}\right),$$

with θ_0 the reference temperature. The modifications to the coefficients B and D due to Kn shows the thermal creep, velocity slip, and temperature jump effects. The continuum solution is recovered as the rarefaction effects diminish (i.e., $\mathrm{Kn} \to 0$).

A quadratic equation for $\frac{\partial T_s}{\partial x}$ can be obtained by combining equations (5.7) and (5.11). The solution for $\frac{\partial T_s}{\partial x}$ for specified heat fluxes is shown in Figure 5.7 as a function of Mach number. Equation (2.22) is used to specify

the Eckert number variation for both the continuum and the rarefied flow cases. The Knudsen number variations are specified by equation (2.21). It is seen that the heat flux required to maintain $\frac{\partial T_s}{\partial x} = 0$ is the same for both continuum and rarefied flow curves. The physical significance of this result is that for a specified Mach number there is only a single value of the heat flux required to compensate the viscous heating effects (see equation (5.11)). Another significant result is the reduction in the magnitude of $\frac{\partial T_s}{\partial x}$ in rarefied flows, which implies that microchannels sustain smaller tangential temperature gradients compared to the large-scale channels. Examining equation (5.7) and Figure 5.7, we see that the volumetric flowrate of a heated microchannel increases due to thermal creep effects. However, cooled microchannels allow less volumetric flowrate compared to the continuum case. If the rarefaction effects are increased further, the viscous heating effects will dominate. Under this condition $\frac{\partial T_s}{\partial x}$ may become positive, which will result in increase of the volumetric flowrate beyond the predictions of continuum theory even for cooled channels.

Temperature profiles under *different* heat flux conditions are shown in Figures 5.8 and 5.9. The temperature jump diminishes if both surfaces of the channel are insulated (see Figure 5.9, top). In this case, the maximum temperature occurs near the walls, where shear stresses are more dominant and the tangential temperature variation becomes positive (see Figure 5.7). This suggests significant changes in the volumetric flowrate of the microchannel, which is the main reason for the differences in the temperature profiles of two cases. Thermal creep in a microchannel can be avoided if the channel is carefully cooled at a cooling rate of $\dot{q} = -\frac{8}{3}\mathrm{PrEc}$ (see equation (5.11)); this results in constant temperature along the channel wall. The temperature distribution for a microchannel, without thermal creep effects, is also given in Figure 5.9 (bottom). This result suggests that the temperature of the insulated surface will be greater than its counterpart modeled by the continuum theory.

The analytical results presented for pressure-driven and shear-driven channels (Section 5.5) are also verified with numerical simulations. Since the temperature variation is in the form of a fourth-order polynomial, convergence of the numerical scheme to the exact solution can be obtained with very coarse discretizations. Typically, fourth-order polynomial expansion in μ**Flow** simulation is sufficient to resolve the spatial variations; see Section 14.1.

Remark: The analytical results presented in this section are based on the incompressibility approximation. Therefore, they are valid for *small* temperature and pressure variations in the microchannels. Small temperature variations can be a good approximation, but it has been shown experimentally that the pressure drop in microchannels could be large. In the experiments of (Pfahler et al., 1991), a total pressure drop of about one order of magnitude is reported. Even though the inlet Mach numbers of

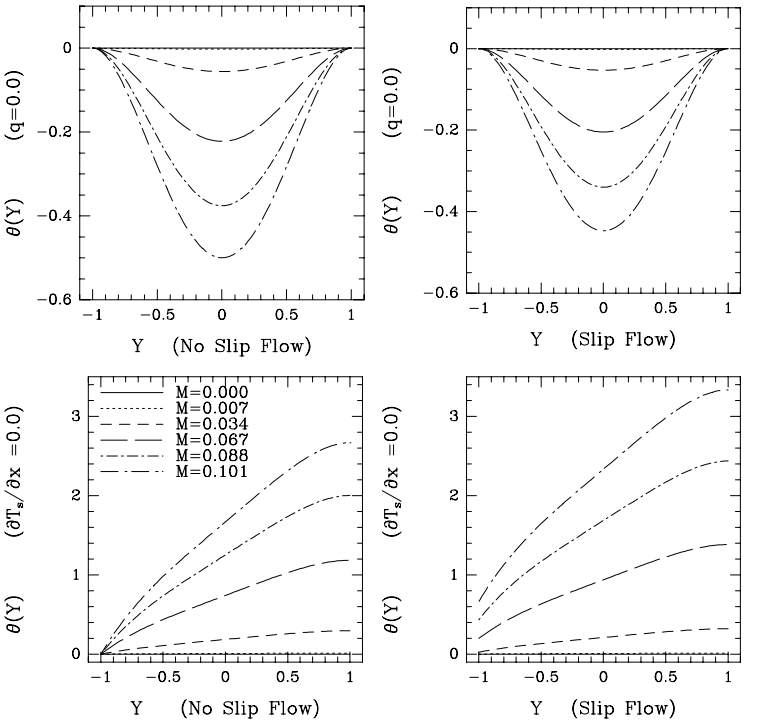

FIGURE 5.9. Temperature profiles in a pressure-driven channel flow for continuum and rarefied flows as a function of Mach number. The top row shows the insulated channel, and the bottom row shows specified heat flux that counterbalances the viscous heating effects, so that overall, $\partial T_s/\partial x = 0$, and therefore there are no thermal creep effects; Re = 1.0 and Pr = 0.7.

the flows are very small, exit Mach numbers up to $M = 0.70$ have been observed. For such situations, the flow in the microchannels cannot be assumed incompressible, and thus the above analysis will not be strictly valid. In general, it is theoretically inconsistent (Aoki, 2001) to use the incompressible flow model with slip boundary conditions caused by rarefaction but the analysis here is meant to highlight approximately the heat transfer effects.

5.4.2 Force-Driven Flows

It is possible to drive channel flows using a body force. The force- and pressure-driven flows are hydrodynamically similar. In either case, the pressure gradient or the force field will be balanced by the viscous shear on the channel walls, and for compressible flows part of the force will be used to

accelerate the fluid in the streamwise direction. However, the two driving forces are very different at the microscopic level. The external force accelerates individual particles, while the pressure gradient induces a collective flow (Zheng et al., 2002). The energy equation for these two cases also shows some differences. For example, the pressure creates a cooling effect by flow expansion (the first term on the right-hand side in equation (2.7)), while the body force affects the kinetic energy of the sytstem (Panton, 1984). For pressure-driven compressible flows the expansion cooling negates the viscous heating (last term in equation (2.7)), while viscous heating may play a crucial role in force-driven flows.

(Zheng et al., 2002) performed extensive DSMC and Navier–Stokes studies of pressure- and force-driven Poiseuille flows in the slip flow regime, and compared these with each other and with the kinetic theory predictions. They have shown that the compressible Navier–Stokes equations do not predict the correct flow physics for the force-driven flow case even for $\mathrm{Kn} = 0.01$ flows. Specifically, the Navier–Stokes solutions failed to predict the central minimum in the temperature profile and the nonconstant pressure distribution. In Figure 5.10 we present the temperature distribution predicted across the channel using the DSMC and Navier–Stokes solutions. The temperature distribution predicted by the Navier-Stokes solution gives a temperature maximum in the center of the channel, while the DSMC and the kinetic theory predicts two off-center maxima, with a local temperature minimum at the center of the channel. The inability of the Navier–Stokes equations to predict this behavior indicates a global failure, which cannot be corrected by modifications of the transport coefficients, equation of state, or the slip/jump boundary conditions. (Zheng et al., 2002) have shown that such discrepancies between the DSMC and Navier-Stokes predictions do not exist for the pressure-driven Poiseuille flow.

The temperature minima can also be predicted using the *entropic* lattice Boltzmann method (LBM), specifically the so-called minimal kinetic model; see Section 15.5. In this nonisorthermal case, the entropic LBM does a good job in capturing the correct temperature variation. Here we present results of (Ansumali et al., 2003), who performed an extensive study of this flow using the 16-velocity minimal kinetic model. The Knudsen number was varied from $\mathrm{Kn} = 0.001$ to $\mathrm{Kn} = 0.5$, while the Mach number was varied from $Ma = 0.01$ to $Ma = 0.3$. Some typical simulation results are presented in Figure 5.4.2. Similar to the DSMC results of (Zheng et al., 2002), the minimal kinetic model predicts the temperature minimum. Some important conclusions, which we can draw from the results of (Ansumali et al., 2003) in Figure 5.4.2 are:

- Even at very low Mach numbers, where the flow is often assumed to be isothermal, the temperature variations can be nonnegligible. For example, the simulation results predict that at $Ma = 0.12, \mathrm{Kn} = 0.2$, the temperature variation can be as large as 7 K within a distance of

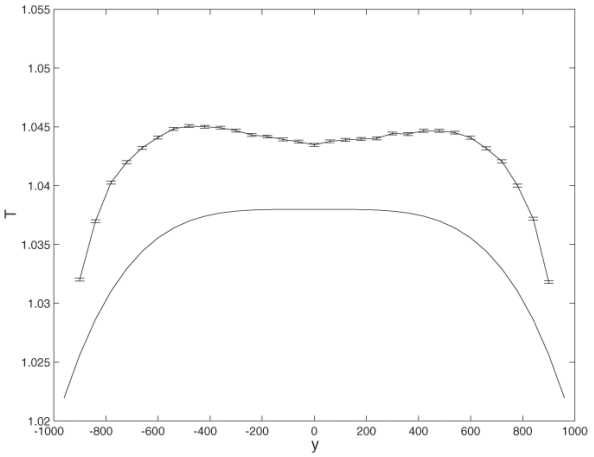

FIGURE 5.10. Temperature profile across a microchannel for the force-driven Poiseuille flow. The curve with the error bars is the DSMC, while the solid line shows the Navier–Stokes results. (Courtesy of A.L. Garcia.)

a few microns.

- The amplitude of the deviation from the isothermal condition is a function of the Knudsen and the Mach number. The deviation increases as the Knudsen or the Mach number increases.
- At a fixed Knudsen number, changing the Mach number does not lead to any qualitative change in the temperature profile.
- At a fixed Mach number the influence of the increase of the Knudsen number is to increase the depth of temperature minimum.
- At a fixed Mach number, as the Knudsen number is increased, the (two symmetric) maxima in the temperature profile move near to the wall.

5.5 Heat Transfer in Couette Microflows

In this section a two-dimensional channel extending from $y = 0$ to $y = h$ is considered. The flow is driven by moving the top wall of the channel with a specified velocity U_0. Thus, this case can be a prototype for a microrotor. Assuming a two-dimensional fully developed flow, the Navier–Stokes equations can be simplified to give linear velocity distribution in the channel. This can be written in nondimensional form

$$\frac{u}{U_0} = U(y/h) = \frac{y/h + \frac{2-\sigma_v}{\sigma_v}\,\mathrm{Kn}}{1 + 2\frac{2-\sigma_v}{\sigma_v}\,\mathrm{Kn}} + \frac{3}{2\pi}\frac{(\gamma-1)}{\gamma}\frac{\mathrm{Kn}^2\,\mathrm{Re}}{\mathrm{Ec}}\frac{\partial T_s}{\partial x}. \qquad (5.13)$$

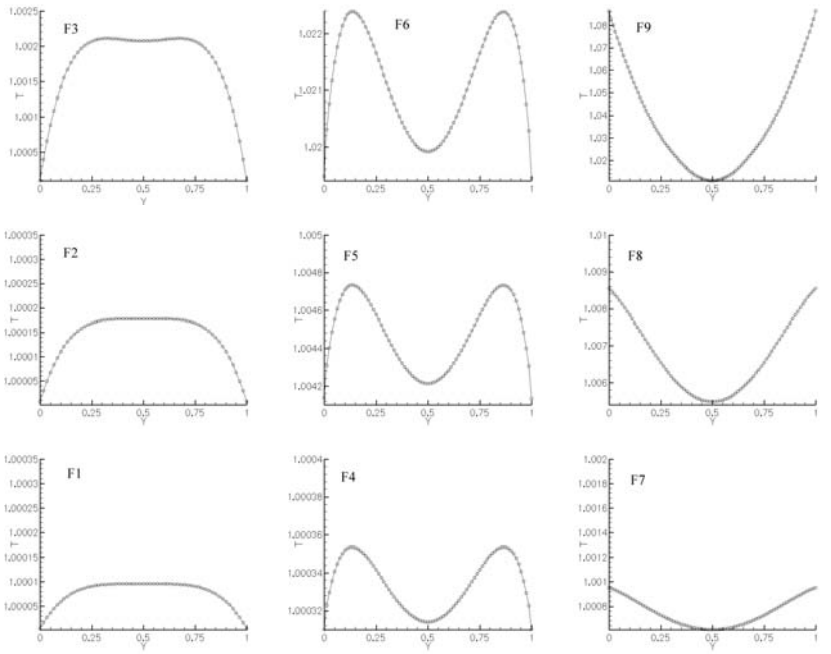

FIGURE 5.11. Temperature profile across the channel as a function of the Knudsen and the Mach numbers. In the figure, the Knudsen number increases going from left to the right, while the Mach number increases going from the bottom to the top. The dimension of the simulated channel was $L/W = 20$. The Knudsen and Mach numbers (Kn, M) used in the simulations were: Plot F1: $(0.001, 0.01)$, Plot F2: $(0.001, 0.02)$, Plot F3: $(0.001, 0.05)$, Plot F4: $(0.20, 0.01)$, Plot F5: $(0.20, 0.05)$, Plot F6: $(0.20, 0.12)$, Plot F7: $(0.45, 0.01)$, Plot F8: $(0.45, 0.04)$, Plot F9: $(0.45, 0.17)$, respectively. (Courtesy of I. Karlin and S. Ansumali.)

The corresponding volumetric flowrate per channel width is

$$\dot{Q} = \frac{1}{2} + \frac{3}{2\pi} \frac{(\gamma - 1)}{\gamma} \frac{\mathrm{Kn}^2 \, \mathrm{Re}}{\mathrm{Ec}} \frac{\partial T_s}{\partial x}. \tag{5.14}$$

It is seen that thermal creep effects result in change of the flowrate of the channel. The ratio of friction coefficients of the shear-driven slip flow to a continuum flow is given by

$$\frac{C_f}{C_{f_0}} = \frac{1}{1 + 2\frac{2-\sigma_v}{\sigma_v} \mathrm{Kn}}. \tag{5.15}$$

The above equation is obtained for constant mass flowrate in the channel. If thermal creep effects are considered, the driving velocity U_o of the channel must be modified to keep the volumetric flowrate constant. Therefore, the

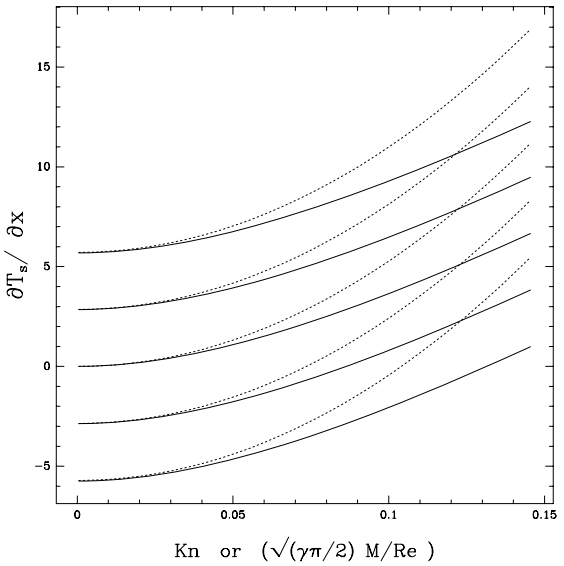

FIGURE 5.12. Variation of tangential temperature gradient ($\frac{\partial T_s}{\partial x}$) along the surface of a shear-driven channel as a function of Mach number for different levels of heat fluxes ($\dot{q}$). Dashed line: continuum; solid line: rarefied. ($\mathrm{Re} = 1.0, \Delta T = 1\,\mathrm{K}$, and $T_0 = 300\,\mathrm{K}$).

thermal creep effects are not included in the derivation of equation (5.15).

Heat convection analysis for a steady and thermally fully developed shear-driven microchannel is obtained by decomposing the temperature profile into two parts, as given in equation (5.10). The channel is assumed to have an insulated top surface and a bottom surface with a specified heat flux ($\dot{q}$). With this decomposition, the temperature variation across the channel becomes a third-order polynomial given by

$$\theta(y) = \frac{A}{6}y^3 + \frac{B}{2}y^2 - \left(\frac{A}{2} + B\right)y + C, \tag{5.16}$$

where

$$A = \frac{\mathrm{RePr}\frac{\partial T_s}{\partial x}}{1 + 2\,\mathrm{Kn}},$$

$$B = \frac{\mathrm{RePr\,Kn}\,\frac{\partial T_s}{\partial x}}{1 + 2\,\mathrm{Kn}} + \frac{3}{2\frac{\partial T_s}{\partial x}}\frac{(\gamma - 1)\,\mathrm{Kn}^2\,\mathrm{Re}^2\mathrm{Pr}}{\gamma}\frac{}{\mathrm{Ec}}\left(\frac{\partial T_s}{\partial x}\right)^2 - \frac{\mathrm{EcPr}}{(1 + 2\,\mathrm{Kn})^2},$$

$$C = \theta_0 - \frac{2\gamma}{\gamma + 1}\frac{\mathrm{Kn}}{\mathrm{Pr}}\dot{q},$$

and

$$\frac{\partial T_s}{\partial x} = \frac{2}{\mathrm{RePr}\dot{Q}}\left[\dot{q} + \frac{\mathrm{EcPr}}{(1 + 2\,\mathrm{Kn})^2}\right]. \tag{5.17}$$

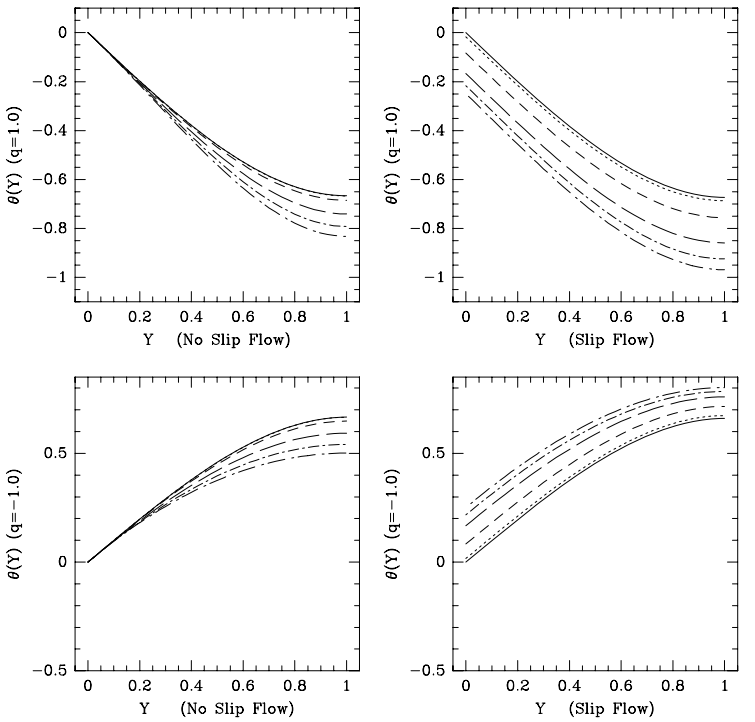

FIGURE 5.13. Variation of temperature profiles in a shear-driven channel flow for continuum and rarefied flows, with specified heat flux at the bottom surface, as a function of Mach number. $Y = 0$ corresponds to a stationary wall, and $Y = 1$ corresponds to a moving wall (Re = 1.0 and Pr = 0.7).

A quadratic equation for $\frac{\partial T_s}{\partial x}$ can be obtained by combining equations (5.14) and (5.17). The solution for $\frac{\partial T_s}{\partial x}$ for specified heat fluxes is shown in Figure 5.12 as a function of Knudsen number. Equation (2.22) is used to specify the Eckert number variation for both the continuum and the rarefied cases. The Knudsen number variations are also specified by equation (2.21). It is seen that the heat flux required to maintain $\frac{\partial T_s}{\partial x} = 0$ for a specified Mach number is smaller in microchannels compared to the continuum case. The viscous heating effects are more dominant in the continuum case compared to microscales; see also (Wendl and Agarwal, 2002). This leads to different results for cooled and heated channels with respect to thermal creep effects.

Variation of temperature profiles across the channel is given in Figure 5.13 as a function of Mach number. Both the continuum and the rarefied flow cases are presented. Here, the nondimensional heat flux of $\dot{q} = \pm 1$ is specified at the bottom surface of the channel. The temperature jump

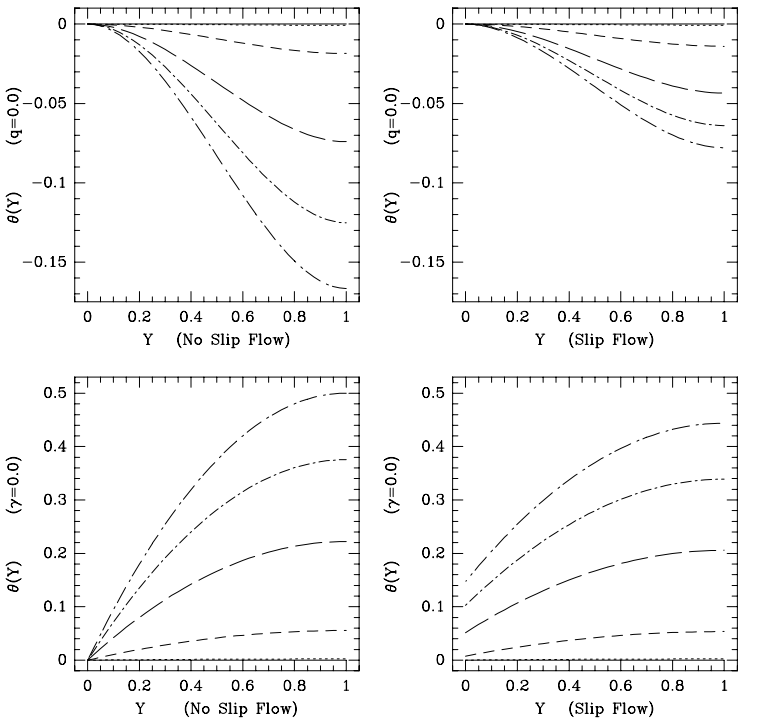

FIGURE 5.14. Variation of temperature profiles in a shear-driven channel flow for continuum and rarefied flows. The top row shows insulated channels, and the bottom row shows cooled channels with equation (5.18) such that there are no thermal creep effects (i.e., $\frac{\partial T_s}{\partial x} = 0$). $Re = 1.0$ and $Pr = 0.7$.

effects are clearly seen in the rarefied flow case. In a microchannel the temperature of the insulated surface is less than that of the continuum predictions for heated channels, while the opposite is true for cooled channels. The effects of thermal creep on volumetric flowrate of the channel depends on the direction that the flow is sheared by the top surface, and whether the channel is cooled or heated. As long as the driving velocity U_0 is in the same direction with increasing $\frac{\partial T_s}{\partial x}$, the volumetric flowrate of the channel will increase due to the thermal creep effects.

The temperature jump diminishes if both surfaces of the channel are insulated (see Figure 5.14, top). For this case, the viscous heating effect in a microchannel is less than the continuum prediction. Therefore, the temperature differences of top and bottom surfaces are relatively small in microchannels compared to the continuum case. It is also possible to specify heat flux on the boundaries that will cancel the viscous heating effects. This case gives zero tangential temperature gradient on the microchannel walls.

The heat flux necessary to maintain this condition is

$$\dot{q} = -\frac{\mathrm{EcPr}}{(1+2\,\mathrm{Kn})^2}. \tag{5.18}$$

The temperature variation for a microchannel without thermal creep effects is also given in Figure 5.14 (bottom). This result suggests that the temperature of the insulated surface will be smaller than its counterpart modeled by the continuum theory.

Remark: The results presented in this section assume *small* temperature and pressure fluctuations compared to the reference pressure and temperature. However, planar shear-driven channels have zero pressure gradient. Thus, the only limitation on the incompressibility assumption is small temperature fluctuations, which is satisfied, since $\Delta T \approx \mathcal{O}(1)$ in this study.